PNAS
www.pnas.org

Supplementary Information for

Precise small molecule cleavage of a r(CUG) repeat expansion in a myotonic dystrophy mouse model

Alicia J. Angelbello[1], Suzanne G. Rzuczek[1], Kendra K. Mckee[2], Jonathan L. Chen[1], Hailey Olafson[2], Michael D. Cameron[3], Walter N. Moss[4], Eric T. Wang[2], and Matthew D. Disney[1,*]

[1]Department of Chemistry, The Scripps Research Institute, 110 Scripps Way, Jupiter, FL 33458
[2]Department of Molecular Genetics & Microbiology, Center for NeuroGenetics, UF Genetics Institute, University of Florida, 2033 Mowry Road, Gainesville, FL 32610
[3]Department of Molecular Medicine, The Scripps Research Institute, 110 Scripps Way, Jupiter, FL 33458
[4]The Roy J. Carver Department of Biochemistry, Biophysics and Molecular Biology, Iowa State University, Molecular Biology Building, 2437 Pammel Drive, Ames, IA 50011-1079
* Author to whom correspondence should be addressed Disney@scripps.edu

This PDF file includes:

www.pnas.org/cgi/doi/10.1073/pnas.1901484116

Supplementary Information Text

General Methods:

Antisense oligonucleotides: Antisense oligonucleotides were purchased from Exiqon Inc. The sequence of the CAG gapmer used is +A+G+CA*G*C*A*G*C*A*G*C*A*+G+C+A and the sequence of the DMPK gapmer used is +A+C+AA*T*A*A*A*T*A*C*C*G*+A+G+G where + indicates locked-nucleic acid modifications and * indicates phosphorothioate modifications.

Synthesis of 2 and 3: Compounds **2** and **3** were synthesized as previously described (1).

Affinity measurements: Affinity measurements of ligands and nucleic acids were performed by monitoring fluorescence intensity as a function of nucleic acid concentration as previously reported (1). Briefly, nucleic acids were annealed in 1× Assay Buffer (8 mM Na_2HPO_4, pH 7.0, 185 mM NaCl and 1 mM EDTA) at 60 °C for 5 min and then cooled to room temperature. Bovine Serum Albumin (BSA) was added to a final concentration of 40 µg/mL. Binding assays with $r(CUG)_{12}$ were completed by titrating the folded RNA into 5 µM **2** in 1× Assay Buffer containing 40 µg/mL BSA. After each addition of RNA, the samples were incubated for 5 min followed by measurement of intrinsic fluorescence intensity of the H RNA binding modules using a BioTek FLX-800 fluorescence plate reader (excitation: 360/40; emission 460/40; sensitivity = 90). Plots of the concentration of nucleic acids versus change in fluorescence were used to determine binding affinity. Curves were plotted in GraphPad Prism and fit using equation 1:

$$y = \frac{(B_{max} * x^h)}{EC_{50}^h + x^h} \qquad \text{(Eq. 1)}$$

Where y is the change in fluorescence; B_{max} is the extrapolated maximum change in fluorescence; x is the concentration of nucleic acid, and h is the Hill slope.

Binding assays with DNA were completed by serial dilutions (1:2) of the DNA in a 5 μM solution of **1** or **2** in 1× Assay Buffer containing 40 μg/mL BSA. The samples were incubated at room temperature for 20 min and fluorescence intensity was measured as described above.

DNA cleavage *in vitro*: The DNA hairpin (5'-GGACCTAGCTTAAAAGCTAGGTCC-3') was purchased from Integrated DNA Technologies, and 500 pmoles was radiolabeled with [γ-^{32}P]ATP using T4 polynucleotide kinase and purified by using a denaturing 15% polyacrylamide gel. The DNA was imaged and excised from the gel and tumbled in 300 mM NaCl for 4 h. Glycogen (0.5 μL; Invitrogen) was added to the solution and the DNA was precipitated with ethanol and resuspended in 40 μL of water. Then, 3 μL of the DNA solution was diluted with 300 μL of 5 mM NaH_2PO_4 (pH 7.4) and heated to 95 °C for 30 s. For competition experiments, a solution of $r(CUG)_{10}$ was separately heated to 95 °C for 30 s. The solutions were cooled to room temperature and varying concentrations of $r(CUG)_{10}$ (6.25, 1.25, 0.312, and 0.063 μM final concentrations) were added to the DNA. Small molecule was added to a final concentration of 250 nM followed by addition of equimolar amount of freshly prepared $(NH_4)_2Fe(SO_4)_2{\cdot}6H_2O$ in 5 mM NaH_2PO_4. The solutions were incubated at 37 °C and supplemented with additional equimolar aliquots of $(NH_4)_2Fe(SO_4)_2{\cdot}6H_2O$ at 30 min and 1 h. The DNA was incubated for 48 h at 37 °C. The reaction was stopped by adding an equal volume of 2× Loading Buffer (8 M urea, 20 mM EDTA, pH 7.5), and the samples were analyzed using a denaturing 20% polyacrylamide gel run at 70 W for 3 h in 1× TBE. Gels were exposed overnight and imaged using a Typhoon 9410 variable mode imager. The percent cleaved was quantified using QuantityOne (BioRad), taking into account the percent cleaved when DNA was treated with Fe^{2+} only (n = 6 for all samples).

Evaluation of compound localization in cells using live-cell fluorescence microscopy: Cells were grown in MatTek 96-well, glass bottom plates, differentiated and treated with 1 μM **2** as

described above. After 24 h, the cells were washed and imaged in 1× DPBS using an Olympus FluoView 1000 confocal microscope at 10×, 20×, and 40× magnification.

Evaluation of pre-mRNA splicing: Cells were grown in 6-well plates and were differentiated and treated or transfected as described in the Methods section. After 48 h, the cells were lysed and total RNA was harvested using a Zymo Quick RNA miniprep kit. Approximately 250 ng of total RNA was reverse transcribed at 50 °C using 100 units of SuperScript III reverse transcriptase (Life Technologies). For mouse muscles, samples were homogenized, total RNA was extracted as described above, and 1 μg of RNA was reverse transcribed. Next, 20% of the RT reaction was subjected to PCR using GoTaq DNA polymerase (Promega). RT-PCR products were observed after 30 cycles of 95 °C for 30 s, 58 °C for 30 s, 72 °C for 1 min and a final extension at 72 °C for 5 min. Products were separated on a 2% agarose gel run at 100 V for 1 h in 1× TBE buffer, visualized by staining with ethidium bromide, and imaged using a Typhoon 9410 variable mode imager. Gels were quantified using ImageJ. Percent rescue was calculated using equation 2.

$$\%\ Rescue = \frac{\%\ exon\ inclusion\ DM1 - \%\ exon\ inclusion\ treated}{\%\ exon\ inclusion\ DM1 - \%\ exon\ inclusion\ WT} * 100 \qquad \text{(Eq. 2)}$$

RT-qPCR analysis of CUG-containing genes: Cells were grown in 100 mm^2 dishes and were differentiated and treated or transfected as described in the Methods. After 48 h, the cells were lysed and total RNA was harvested using a Zymo Quick RNA miniprep kit. For mouse muscles, samples were homogenized and total RNA was extracted using an Omni handheld tissue homogenizer and TRIzol. The RNA was cleaned up using Zymo Quick RNA miniprep kit with an on-column DNase. Approximately 1 μg of total RNA was reverse transcribed using a qScript cDNA synthesis kit (20 μL total reaction volume, Quanta BioSciences); 2 μL of the RT reaction was used for each primer pair for qPCR with SYBR Green Master Mix performed on a 7900HT Fast Real-Time PCR System. Relative abundance of each transcript was determined by

normalizing to *GAPDH* for RNA isolated from cells and *18S* for RNA isolated from *HSA*^{LR} mice. *GAPDH* levels were chosen for normalization for cellular studies as they are similar to those of DMPK. Likewise, 18S rRNA levels were chosen for normalization in HSA^{LR} mice as they are similar to the levels of the r(CUG)$_{exp}$-containing transgene.

Evaluation of nuclear foci using fluorescence in situ hybridization (FISH): RNA-FISH to image nuclear foci was completed as previously described (1). Cells were grown in a MatTek 96-well glass bottom plate and differentiated and treated as described above. After 48 h, cells were fixed followed by FISH as previously described using 1 ng/μL DY547-2'OMe-(CAG)$_6$. Immunostaining of MBNL1 was completed as previously described using the MB1a antibody (diluted 1:4), which was generously supplied by Prof. Glenn E. Morris (Wolfson Centre for Inherited Neuromuscular Disease)(2), and goat anti-mouse IgG-DyLight 488 conjugate (1:2000 dilution). Nuclei were stained using a 1 μg/μL solution of DAPI in 1× DPBS. Cells were imaged in 1× DPBS using an Olympus FluoView 1000 confocal microscope at 100× magnification. The number of r(CUG)^{exp}-MBNL1 foci were counted in 40 nuclei/replicate (120 total nuclei counted over three replicates).

Evaluation of γ-H2AX foci: Effects of small molecules on DNA double strand breaks in cells were assessed using γ-H2AX immunofluorescence. Cells were grown, fixed, and washed as described above. After washing with 2× SCC for 30 min at 37 °C, cells were incubated with a 1:500 dilution of anti-γH2AX (Abcam) at 37 °C for 1 h. Cells were then washed 3 times with 1× DPBS containing 0.1% Triton X-100 (v/v) for 5 min at 37 °C followed by incubation with a 1:200 dilution of goat anti-mouse IgG-DyLight 488 conjugate (Thermo Scientific) at 37 °C for 1 h. After washing three times with 1× DPBS containing 0.1% Triton X-100 (v/v) and 2 times with 1× DPBS for 5 min at 37 °C, nuclei were stained with DAPI (1 μg/mL). Cells were imaged in 1× DPBS

using an Olympus FluoView 1000 confocal microscope at 100× magnification. The number of γ-H2AX foci were counted in 40 nuclei/replicate (120 total nuclei counted over three replicates).

DMPK Measurements: A pharmacokinetics (PK) assessment was used to profile **2**'s PK properties. Four C57BL/6 mice were dosed *i.p.* with 10 mg/kg of **2**. Blood draws (25 μL) were taken at the indicated time points. Compound levels were determined by liquid chromatography/MS-MS using a QTRAP 5500 LC-MS/MS System (AB Sciex).

Treatment of *HSA*^{LR} and FVB mice: Gender and age-matched mice (5 weeks old) were used for *in vivo* studies. Compounds **1** and **2** were suspended in 1× DPBS, and mice were administered 10 mg/kg **1** or **2** by i.p. injection every other day for 1 week (4 total injections). Vehicle injections consisted of 200 μL injections of 1× DPBS. Myotonia was assessed on day 8.

Electromyography: Myotonia was assessed via electromyography (EMG) after a week of treatment as previously described (44). The EMG experiments were performed under general anesthesia (isoflurane) using 30 grade concentric needle electrodes with at least 15 needle insertions per muscle. Myotonia was assessed in the right tibialis anterior, gastrocnemius, and quadriceps muscle, and all samples were blinded. Myotonic discharges were recorded as a percentage of the total number of insertions.

Chloride ion channel (CLCN1) immunostaining in *HSA*^{LR} mice: CLCN1 protein was detected in mouse TA muscle sections using immunofluorescence. Frozen TA muscles were sectioned into 5 μm slices and fixed with 10% neutral buffered formalin at room temperature for 15 min. Sections were washed with 1× PBS and incubated with 1% normal donkey serum for 1 h. Sections were then incubated with a 1:100 dilution of rabbit anti-rat Clcn1 (Alpha Diagnostic International) in

1% donkey serum at 4 °C overnight. Sections were washed with 1× PBS and incubated with a 1:500 dilution of donkey anti-rabbit Alexa Fluor488 (Life Technologies) for 2 h at room temperature. Sections were washed with 1× PBS and mounted with ProLong Gold Antifade Mountant with DAPI (Life Technologies) and imaged using an Olympus FluoView 1000 confocal microscope at 10× magnification.

RNA-seq: Total RNA was prepared for RNA-Seq libraries using the NEB Ultra II Kit with ribosomal RNA depletion. Libraries were sequenced in the NextSeq 500 v2 using paired end, 2x75 kits. Raw fastq was demultiplexed and mapped to the mm10 build of the mouse genome by Hisat2 (3). Gene expression changes were estimated by Kallisto and Sleuth (4,5). Splicing Ψ values were estimated by MISO (6) using the version 2 build of mm10 MISO annotations for skipped exons, alternative splice sites, retained introns, and mutually exclusive exons. To determine splicing events significantly regulated between *HSA*^{LR} and wild-type mice, a monotonicity test (7) was used in which minimum ΔΨ was 0.1 and minimum Z-value was 1.8. Custom Python scripts were written to perform downstream analyses. Composite scores were generated from splicing events that have > 0.25 |ΔΨ| between WT and *HSA*^{LR} mice and consistency across replicates (|Z| > 1.4).

Prediction of conserved RNA structures: RNA sequences were folded in 150 nt windows every 10 nts from the 5′ end using RNAfold of the ViennaRNA software package (8). The free energy of each window was calculated and compared to the average free energy of a set of 50 randomized sequences for the same window using a z-score of the difference between the free energies. Windows with z-scores more than one standard deviation below the average z-score were considered likely to form stable structures. Sequences from these windows were then compiled and refolded to generate a new set of structures. NCBI Blast was used to query and align sequences in predicted structured regions with sequence fragments in non-human primates (9). Resulting

sequence fragments were filtered to remove duplicates and fragments 80% of the length of the query sequence. Sequences were aligned using MAFFT and folded using RNAalifold to generate a consensus structure (8,10). Base pairs in each aligned sequence and the consensus structure were counted. The percent of canonical base pairs for each base pair coordinate was calculated and averaged for the entire structure.

Analysis of RNA secondary structure probability: For probability calculations, RNA sequences containing CUG loops in their predicted secondary structures were folded in RNA Structure (Version 6.0.1, Mathews Lab). The top 20 predicted structures were analyzed and the percentage of structures containing the predicted number of CUG loops was calculated. Additionally, regions of CUG repeats from each sequence were folded separately and their free energies were calculated using RNAStructure.

Evaluation of hydroxyproline content in the lungs of *HSA*$^{\mathbf{LR}}$ mice: Lung hydroxyproline concentrations were measured using Hydroxyproline Assay Kit (Sigma) per the manufacturer's recommended protocol using the manufacturer's provided standards.

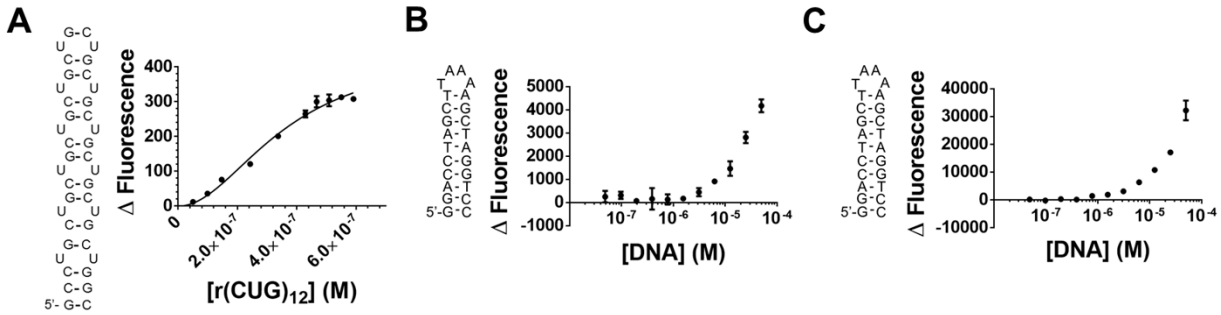

Fig. S1. Binding of **1** and **2** to r(CUG)$_{12}$ and a DNA hairpin. The secondary structures of the constructs used are show to the left of each plot. (*A*) Representative analysis of **2** binding to r(CUG)$_{12}$ where the EC_{50} is 365 ± 75 nM. (*B*) Representative binding analysis of **1** to DNA where the EC_{50} is greater than 50 μM. (*C*) Representative binding analysis of **2** to DNA where the EC_{50} is greater than 50 μM.

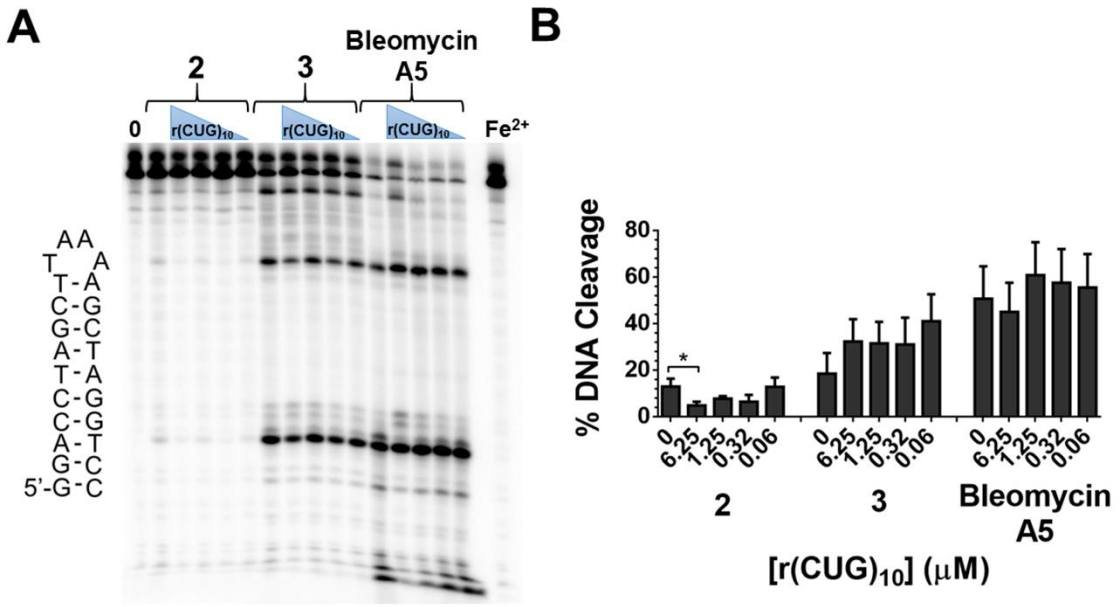

Fig. S2. Studies of DNA cleavage *in vitro*. (*A*) Representative gel image of DNA treated with 250 nM **2**, **3**, or bleomycin with or without $r(CUG)_{10}$ as a competitor. Zero represents untreated DNA and Fe^{2+} represents DNA treated with $(NH_4)_2Fe(SO_4)_2{\cdot}6H_2O$. (*B*) Quantification of average DNA cleavage *in vitro*, where only cleavage by **2** is significantly affected by competitor $r(CUG)_{10}$. Zero indicates that no competitor $r(CUG)_{10}$ was added. Note: % DNA Cleavage values account for the percentage of cleavage observed when DNA is incubated with Fe^{2+} only. Error bars represent SD; n = 6 biological replicates; $^*P < 0.05$ as determined by a 1-way ANOVA.

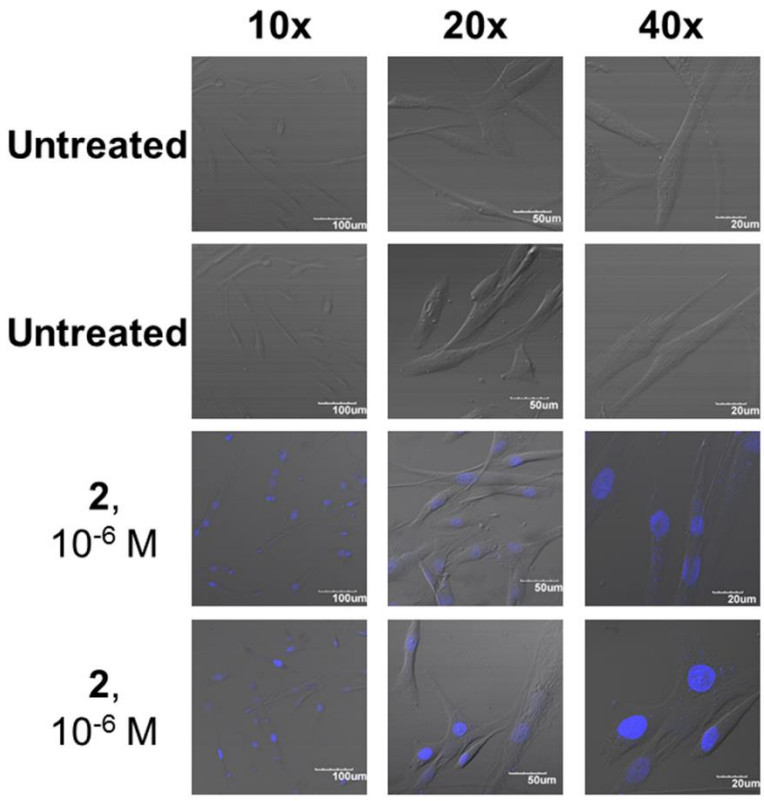

Fig. S3. Representative live cell images of untreated or **2**-treated DM1 myotubes. DIC images were overlaid with fluorescence images (derived from the inherent fluorescence of **2**) and were taken at 10×, 20×, and 40× magnification.

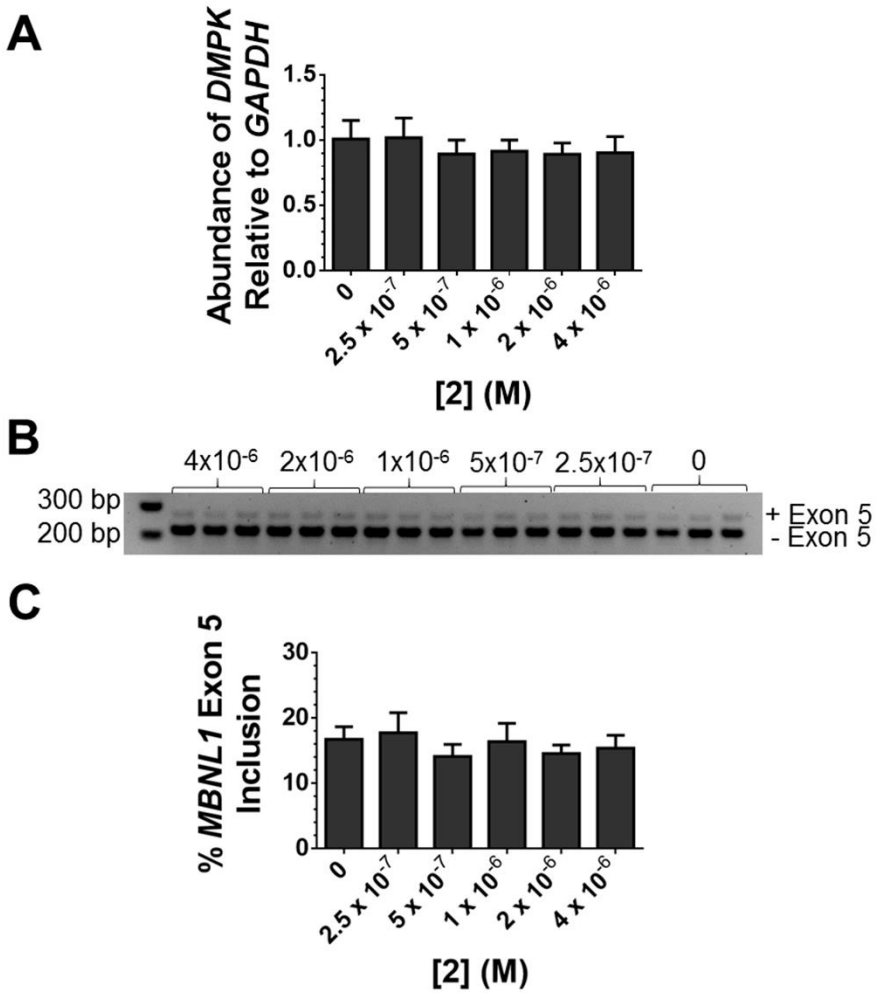

Fig. S4. Evaluation of **2** in WT myotubes. (*A*) RT-qPCR analysis of *DMPK* abundance in WT myotubes treated with **2**. Error bars represent SD; n = 3. (*B*) Representative gel image of *MBNL1* exon 5 splicing in WT myotubes treated with **2**. (*C*) Quantification of *MBNL1* exon 5 splicing. Error bars represent SD; n = 3 biological replicates.

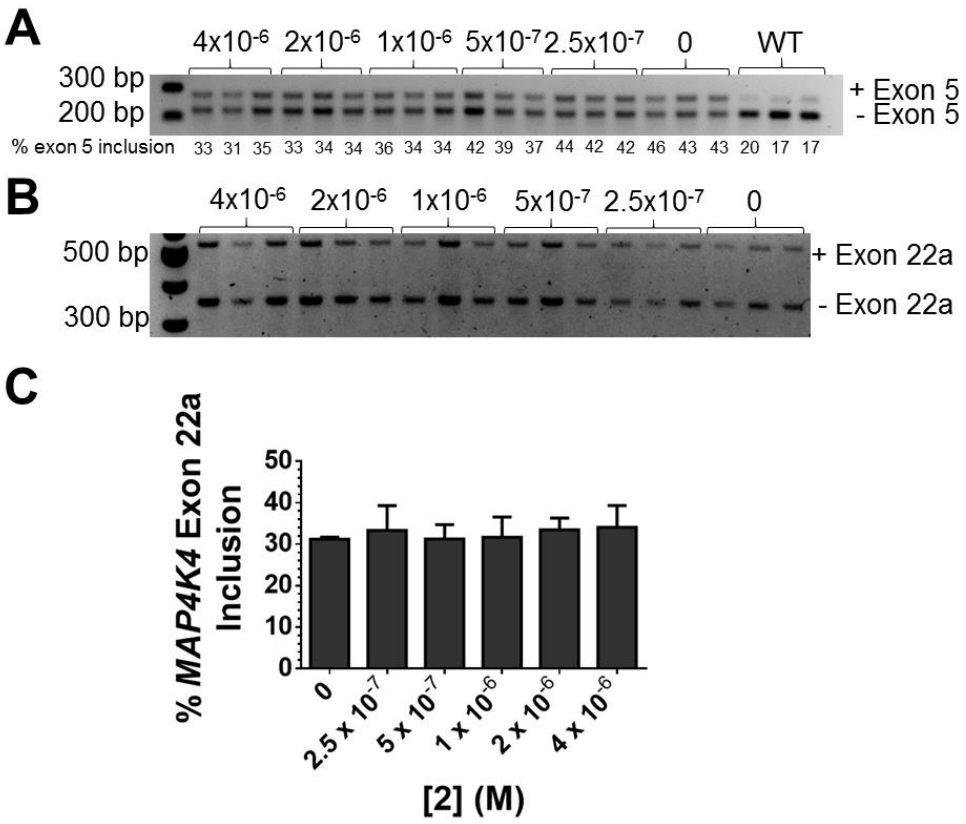

Fig. S5. Evaluation of **2** in DM1 myotubes. (*A*) Representative gel image of *MBNL1* splicing in DM1 myotubes treated with **2**. (*B*) Representative gel image of *MAP4K4* exon 22a splicing (NOVA-regulated) in DM1 myotubes treated with **2**. (*C*) Quantification of *MAP4K4* exon 22a splicing. Error bars represent SD; n = 3 biological replicates.

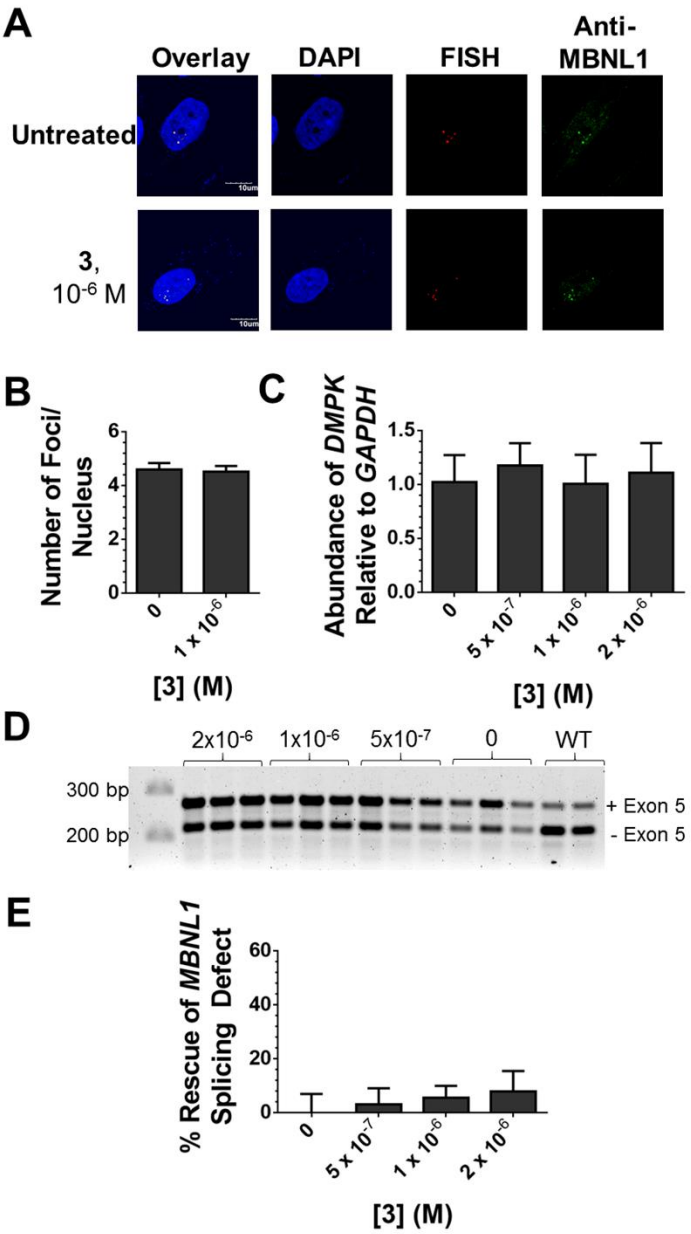

Fig. S6. Evaluation of **3** in DM1 myotubes. (*A*) Representative images from RNA-FISH experiments to assess nuclear foci. (*B*) Quantification of nuclear foci. Error bars represent SD; n = 3 biological replicates, 40 nuclei counted per replicate. (*C*) RT-qPCR of *DMPK* abundance in DM1 myotubes treated with **3**. Error bars represent SD; n = 3 biological replicates. (*D*) Representative gel image of *MBNL1* exon 5 splicing in DM1 myotubes treated with **3**. (*E*) Quantification of *MBNL1* exon 5 splicing defect. Error bars represent SD; n = 3 biological replicates.

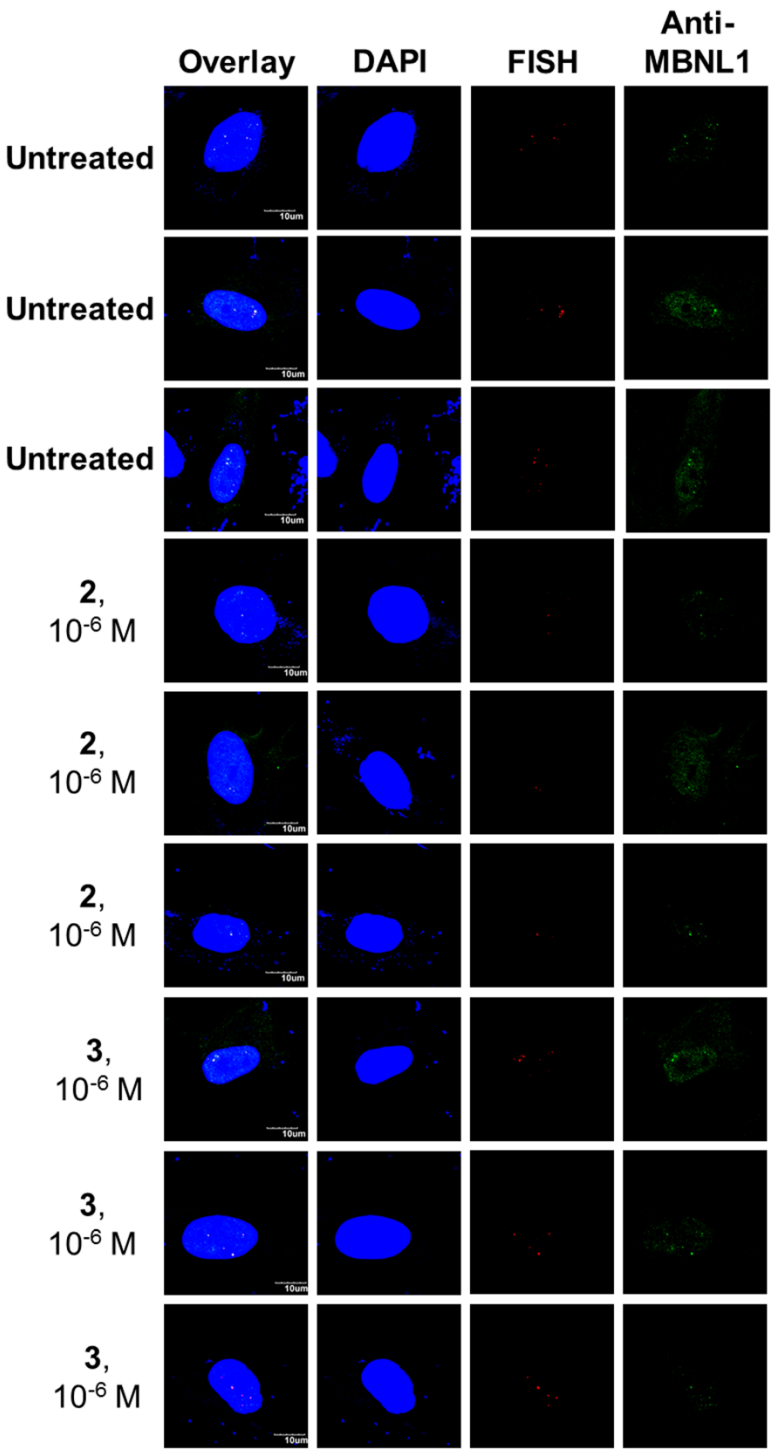

Fig. S7. Additional representative images from RNA-FISH experiments in untreated, **2**-treated, and **3**-treated cells to assess their ability to inhibit formation of nuclear foci.

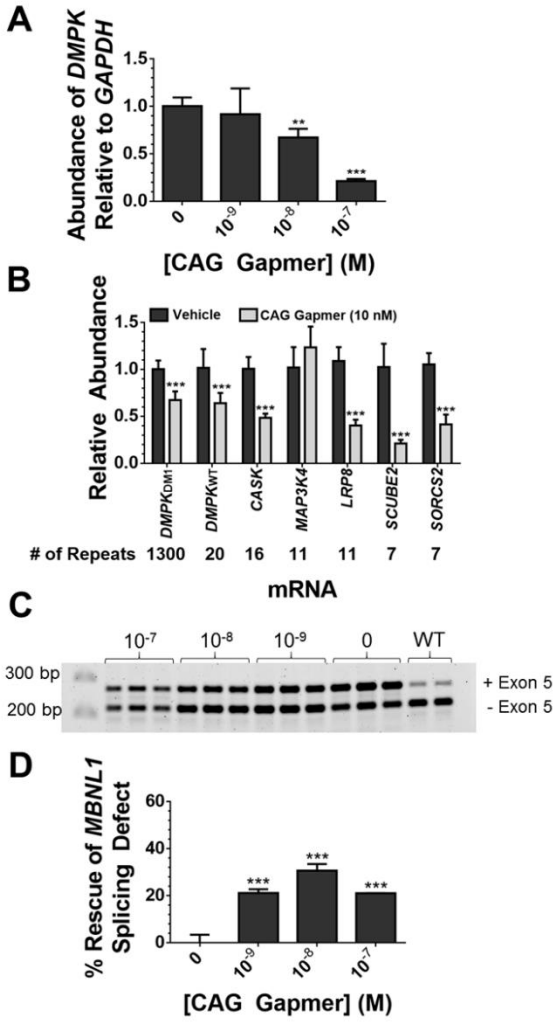

Fig. S8. Evaluation of CAG gap-mer in DM1-affected myotubes. (*A*) RT-qPCR analysis of *DMPK* abundance in DM1 myotubes transfected with CAG gap-mer. Error bars represent SD, n = 3 biological replicates, **P < 0.01, ***$P < 0.001$ (1-way ANOVA). (*B*) RT-qPCR analysis of CUG-containing mRNAs in DM1 myotubes transfected with 10 nM CAG gap-mer. Dark gray bars represent vehicle-treated cells and light gray bars represent cells treated with 10 nM CAG gapmer. Error bars represent SD, n = 3 biological replicates, ***$P < 0.001$ (*t*-test). (*C*) Representative gel image of *MBNL1* exon 5 splicing in DM1 myotubes transfected with CAG gap-mer. (*D*) Quantification of rescue of *MBNL1* exon 5 splicing defect in DM1 myotubes transfected with CAG gap-mer. Error bars represent SD, n = 3 biological replicates, ***$P < 0.001$ (1-way ANOVA).

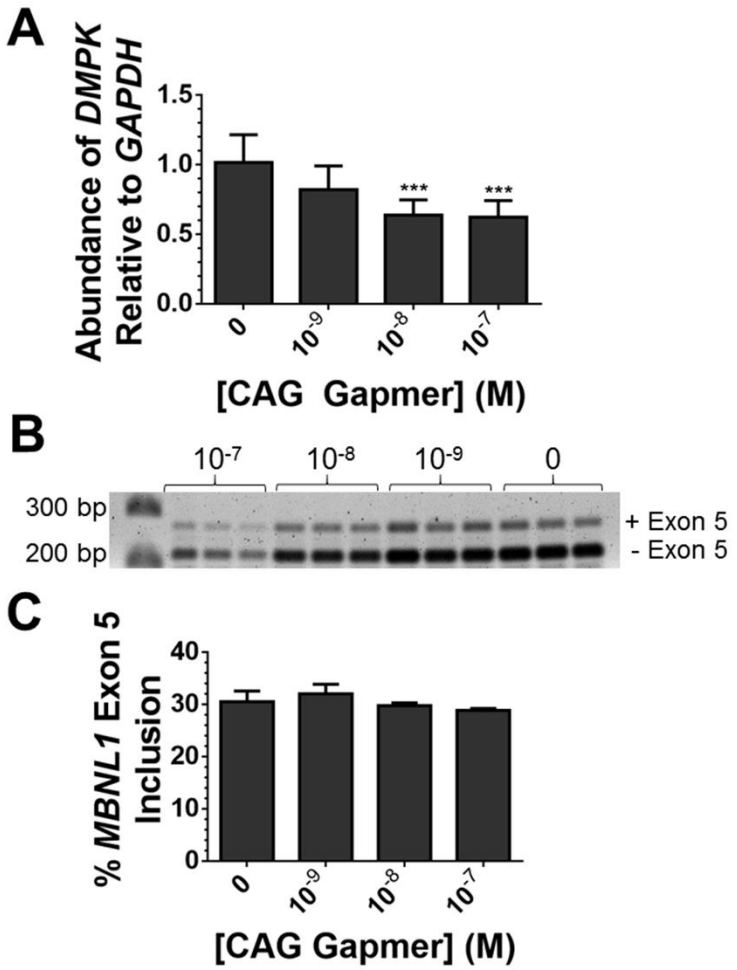

Fig. S9. Evaluation of CAG gap-mer in WT myotubes. (*A*) RT-qPCR analysis of *DMPK* abundance in WT myotubes treated with CAG gap-mer. Error bars represent SD, n = 3 biological replicates, ***$P < 0.001$ (1-way ANOVA). (*B*) Representative gel image of *MBNL1* exon 5 splicing in WT myotubes treated with CAG gap-mer. (*C*) Quantification of *MBNL1* exon 5 splicing. Error bars represent SD, n = 3 biological replicates.

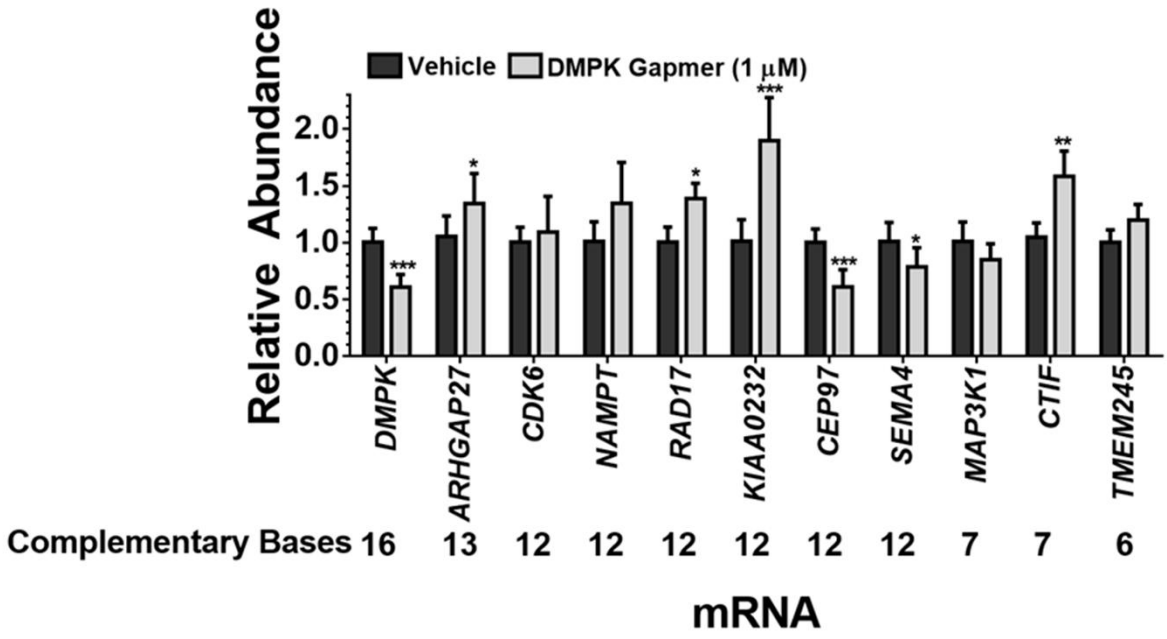

Fig. S10. Evaluation of the selectivity of a gap-mer targeting a non-repeating sequence in *DMPK* mRNA in DM1 myotubes. *DMPK* gap-mer selectivity was analyzed at 1 μM. Dark gray bars represent vehicle-treated cells while light gray bars represent cells treated with 1 μM of the *DMPK* gap-mer. Error bars represent SD; n = 3 biological replicates. **P* < 0.05, ***P* < 0.01, ****P* < 0.001 (*t*-test).

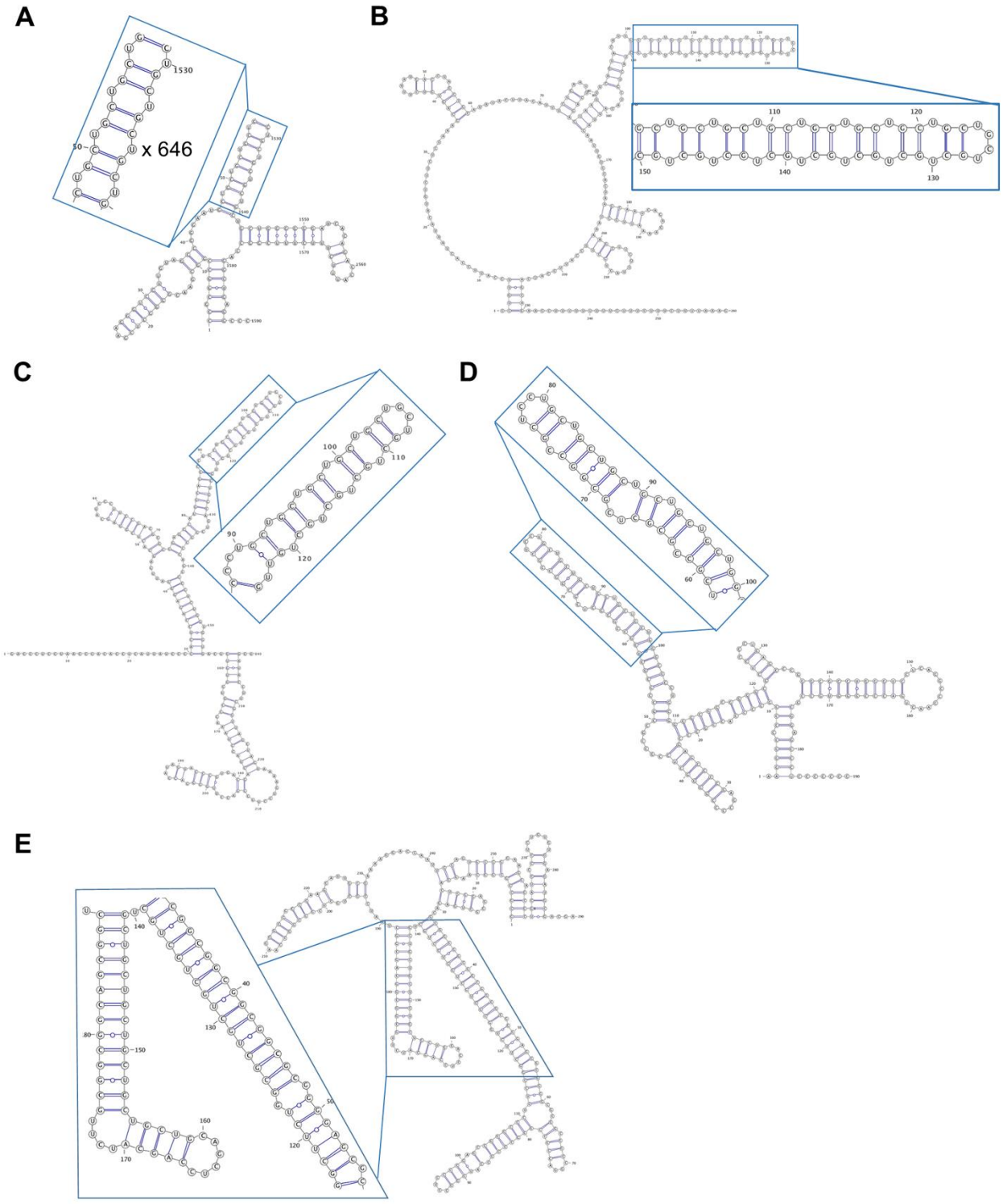

Fig. S11. RNA secondary structures for all transcripts expressed in myotubes that have greater than six repeats of r(CUG). (*A*) Structure of the mutant *DMPK* containing r(CUG)^{exp}. (*B*) Structure of *CASK* with 16 r(CUG) repeats. (*C*) Structure of *MAP3K4K* with 11 r(CUG) repeats. (*D*)

Structure of *SORCS2* with 7 r(CUG) repeats. (*E*) Structure of *LRP8* RNA with 11 r(CUG) repeats. Note: wild type *DMPK* (15 r(CUG) repeats) and *SCUBE2* (7 r(CUG) repeats) did not fold into a stable structure.

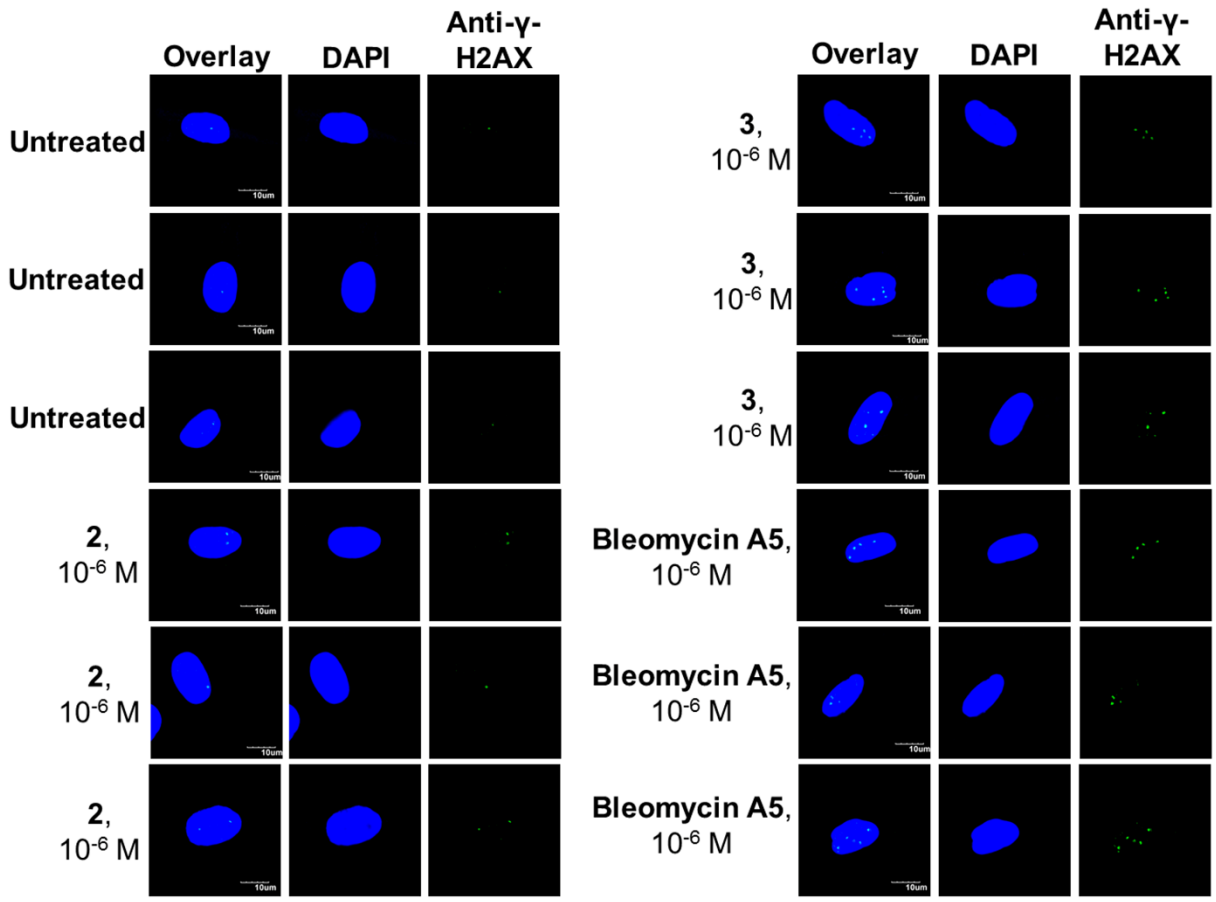

Fig. S12. Additional representative images of γ-H2AX immunostaining in untreated, **2**-treated, **3**-treated, and bleomycin A5-treated cells.

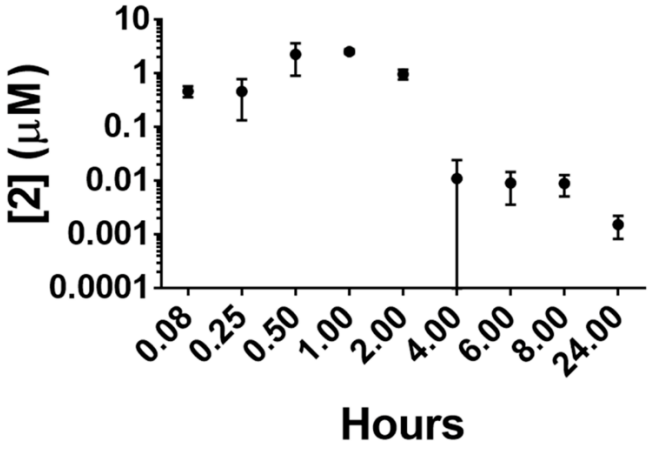

Fig. S13. Amount of **2** present in plasma as a function of time after *i.p.* injection of 10 mg/kg **2** in C57BL/6 mice.

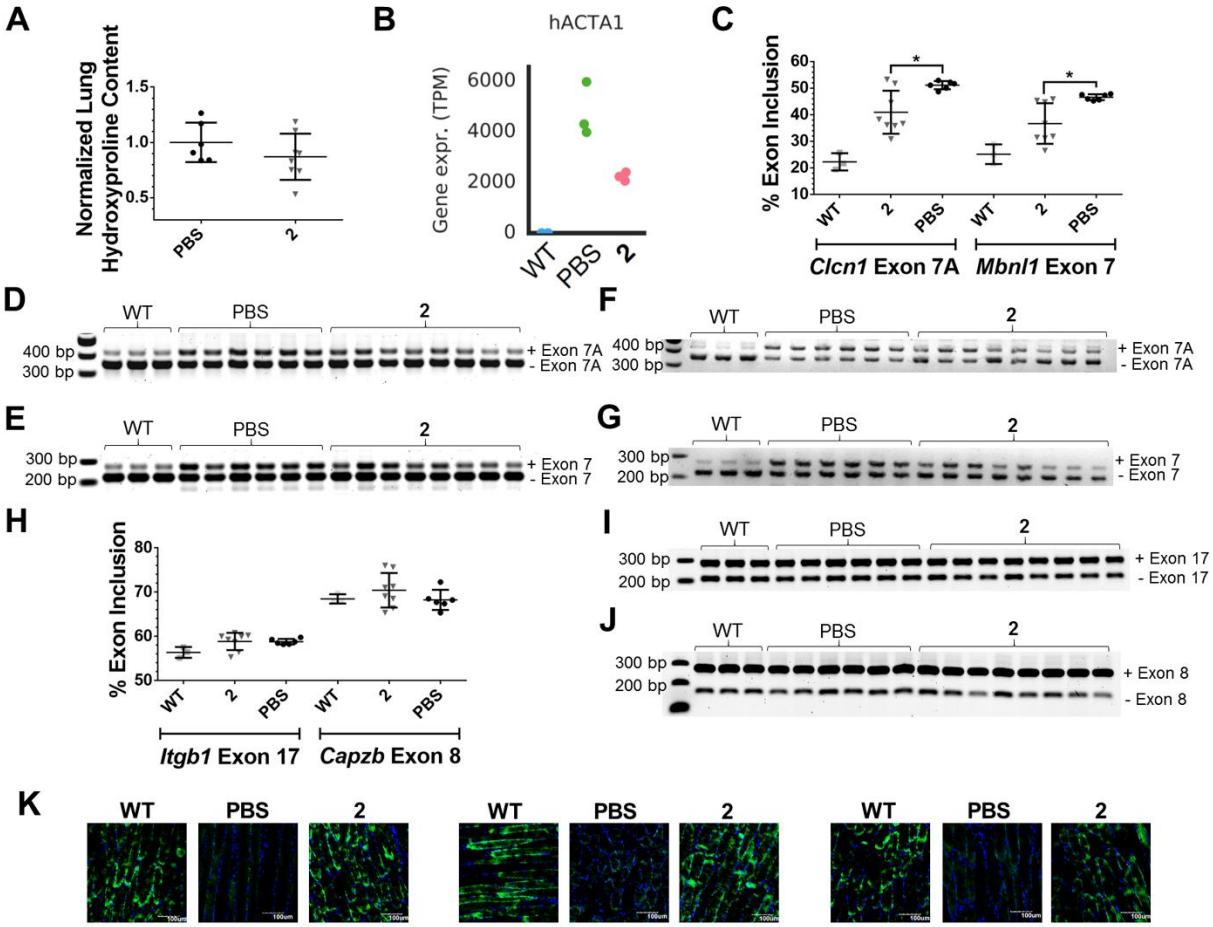

Fig. S14. Evaluation of **2** in *HSA*^{LR} mice. (*A*) Lung hydroxyproline concentrations in *HSA*^{LR} mice treated with **2**. Error bars represent SD; n = 6 mice for vehicle-treated and n = 8 mice for **2**-treated. (*B*) Gene expression of r(CUG)$_{250}$-containing *hACTA1* transgene determined by RNA-seq. (*C*) Quantification of RT-PCR analysis of *Clcn1* exon 7A and *Mbnl1* exon 7 splicing in gastrocnemius muscle of *HSA*^{LR} mice. Error bars represent SD. **P* < 0.05 (1-way ANOVA), n = 3 mice for wild-type, n = 6 mice for vehicle-treated, n = 8 mice for **2**-treated. (*D*) Representative gel image of RT-PCR analysis of *Clcn1* Exon 7a splicing in TA muscle. (*E*) Representative gel image of RT-PCR analysis of *Mbnl1* Exon 7 splicing in TA muscle. (*F*) Representative gel image of RT-PCR analysis of *Clcn1* Exon 7a splicing in gastrocnemius muscle. (*G*) Representative gel image of RT-PCR analysis of *Mbnl1* Exon 7 splicing in gastrocnemius muscle. (*H*) Quantification of RT-PCR analysis of *Itgb1* and *Capzb* splicing (non-MBNL1 regulated) in TA muscle of *HSA*^{LR} mice. Error

bars represent SD; n = 3 mice for wild-type, n = 6 mice for vehicle-treated, and n = 8 mice for **2**-treated. (*I*) Representative gel image of RT-PCR analysis of *Itgb1* Exon 17 splicing. (*J*) Representative gel image of RT-PCR analysis of *Capzb* Exon 8 splicing. (*K)* Additional representative images of CLCN1 immunostaining in TA muscle sections of WT, PBS-treated, and **2**-treated mice.

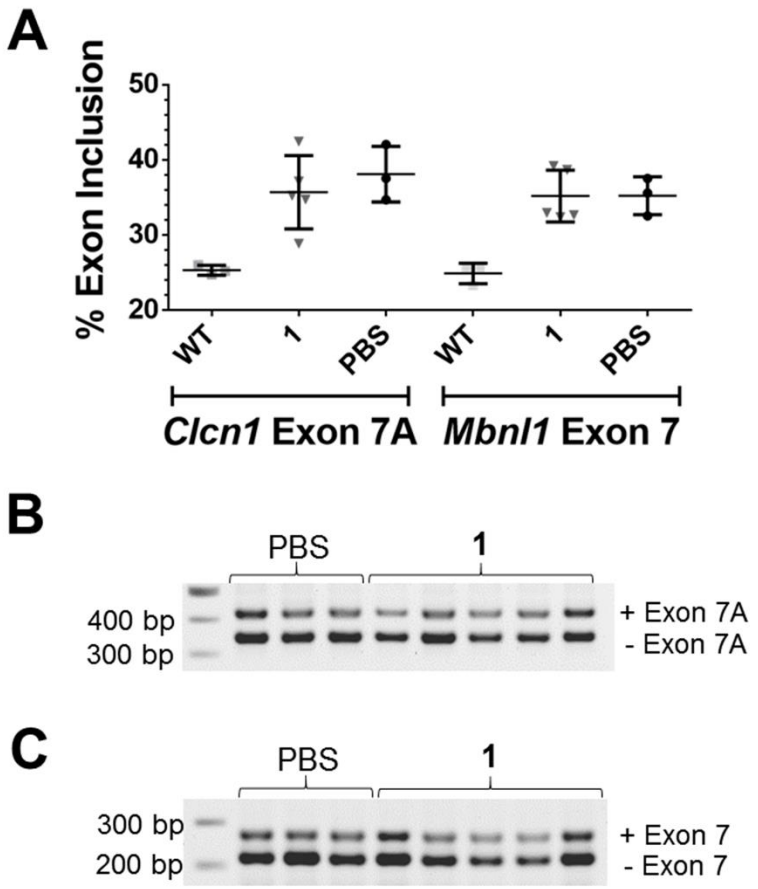

Fig. S15. Evaluation of **1** in *HSA*^{LR} mice. (*A*) Quantification of RT-PCR analysis of *Clcn1* exon 7A and *Mbnl1* exon 7 splicing in TA muscle of *HSA*^{LR} mice treated with **1**. Error bars represent SD; n = 3 mice for WT, n = 5 mice for **1**-treated, and n = 3 mice for PBS. (*B*) Representative gel image of RT-PCR analysis of *Clcn1* Exon 7a splicing in TA muscle. (*C*) Representative gel image of RT-PCR analysis of *Mbnl1* Exon 7 splicing in TA muscle.

Table S1. Summary of RNA secondary structure prediction.

Gene	# of CUG Repeats	Predicted to form CUG structure	# of CUG loops	Base-pair conservation	Evolutionarily Conserved	Probability of loop formation	ΔG° of r(CUG) repeat formation (kcal mol^{-1})
DMPK WT	20	No	N/A	96%	Yes	N/A	−25.1
DMPK CUG_{1300}	1300	Yes	649	N/A	N/A	95%	−1945.1
CASK	16	Yes	7	89%	Yes	47%	−19.1
MAP3K4	11	Yes	4	96%	Yes	30%	−10.1
LRP8	11	No	N/A	97%	Yes	N/A	−10.1
SORCS2	7	No	N/A	98%	Yes	N/A	−4.1
SCUBE2	7	No	N/A	94%	Yes	N/A	−4.1

Table S2. Sequences of primers used for RT-qPCR and qPCR.

Gene	Forward Primer (5'-3')	Reverse Primer (5'-3')	Purpose
MBNL1	GCTGCCCAATACCAGGTCAAC	TGGTGGGAGAAATGCTGTATGC	RT-PCR
MAP4K4	CCTCATCCAGTGAGGAGTCG	ATCACAGGAAAATCCCACCA	RT-PCR
DMPK	CGTGCAAGCGCCCAG	CTCCACCAACTTACTGTTTCATCCT	qPCR
CASK	TTGAAATCGTAAAGCGAGCTGA	CAGTAGCGTAGAGCTTCCAGTA	qPCR
MAP3K4	CAATAAGCCTTACCTCAGCCTTG	GTTAAGCCAGAAACCAGACGTA	qPCR
LRP8	GCCAAGGATTGCGAAAAGGAC	GTGGTCTAAGCAGTCATCGTC	qPCR
SORCS2	CACGTCGTTCGTGCTCAAG	CGTCCCGAAATCTGATGACCG	qPCR
SCUBE2	CCCACCTCCTACAAGTGCTC	TGCAACGATAATTGCCTGGAAT	qPCR
GAPDH	AAGGTGAAGGTCGGAGTCAA	AATGAAGGGGTCATTGATGG	qPCR
18S	GTAACCCGTTGAACCCCATT	CCATCCAATCGGTAGTAGCG	qPCR
ARHGAP27	GATGGCGGCGGACGTG	GTCCTTGCCGGTGTACTCG	qPCR
CDK6	CTGAATGCTCTTGCTCCTTT	AAAGTTTTGGTGGTCCTTGA	qPCR
NAMPT	GGACCCAGTTGCTGATCCC	TTCCCTGCTGGCGTCCTAT	qPCR
RAD17	ACACGCTCTTTACTCAGGGAA	AGCATATCCTCGGGCTTTGTT	qPCR
KIAA0232	ACTTCCTCTCCTAAGGACTGC	CATGCACAGTGGTGGGTACT	qPCR
CEP97	ATGGCACCTGCTTACCTACC	ACTCTGAGGTTTAGGCACCAG	qPCR
SEMA4	TCCAATCTCTGAGGCTGACTC	GGGATAAAGCGAAGATGGTGTC	qPCR
MAP3K1	TCTCACCATATAGCCCTGAGGA	AGGAAAGAGTTAGGCCCTATCTG	qPCR
CTIF	AGACCATGACCATCGAGAACC	ACGTTTTGTCTCAACCTCTGG	qPCR
TMEM245	TGCAGTCTGGATACTCAAAAAGC	CCACACATGGTAGCGTTTCTCTA	qPCR
HSA	GACGAGGCTCAGAGCAAGAGA	TGATGATGCCGTGCTCGATA	qPCR
Clcn1	TGAAGGAATACCTCACACTCAAGG	CACGGAACACAAAGGCACTG	RT-PCR
Mbnl1	GCTGCCCAATACCAGGTCAAC	TGGTGGGAGAAATGCTGTATGC	RT-PCR
Itgb1	CCTACTGGTCCCGACATCATC	CTTCGGATTGACCACAGTTGTC	RT-PCR
Capzb	GCACGCTGAATGAGATCTACTTTG	CCGGTTAGCGTGAAGCAGAG	RT-PCR

References

1. S. G. Rzuczek *et al.*, Precise small-molecule recognition of a toxic CUG RNA repeat expansion. *Nat Chem Biol* **13**, 188-193 (2017).
2. I. Holt *et al.*, Defective mRNA in myotonic dystrophy accumulates at the periphery of nuclear splicing speckles. *Genes Cells* **12**, 1035-1048 (2007).
3. D. Kim, B. Langmead, S. L. Salzberg, HISAT: a fast spliced aligner with low memory requirements. *Nat Methods* **12**, 357 (2015).
4. N. L. Bray, H. Pimentel, P. Melsted, L. Pachter, Near-optimal probabilistic RNA-seq quantification. *Nat Biotech* **34**, 525 (2016).
5. H. Pimentel, N. L. Bray, S. Puente, P. Melsted, L. Pachter, Differential analysis of RNA-seq incorporating quantification uncertainty. *Nat Methods* **14**, 687-690 (2017).
6. Y. Katz, E. T. Wang, E. M. Airoldi, C. B. Burge, Analysis and design of RNA sequencing experiments for identifying isoform regulation. *Nat Methods* **7**, 1009-1015 (2010).
7. E. T. Wang *et al.*, Antagonistic regulation of mRNA expression and splicing by CELF and MBNL proteins. *Genome Res* **25**, 858-871 (2015).
8. R. Lorenz *et al.*, ViennaRNA Package 2.0. *Algorithm Mol Biol* **6**, 26 (2011).
9. S. F. Altschul, W. Gish, W. Miller, E. W. Myers, D. J. Lipman, Basic local alignment search tool. *J Mol Biol* **215**, 403-410 (1990).
10. S. Kuraku, C. M. Zmasek, O. Nishimura, K. Katoh, aLeaves facilitates on-demand exploration of metazoan gene family trees on MAFFT sequence alignment server with enhanced interactivity. *Nucleic Acids Res* **41**, W22-W28 (2013).